Molecular Catalysis 494 (2020) 111114

Contents lists available at ScienceDirect

Molecular Catalysis

journal homepage: www.elsevier.com/locate/mcat

Zn-doped W/aluminium oxide catalyst: Efficient strategy towards sustainable oxidation of alcohols

Menglu Cai[a], Jun Li[b], Xiaozhong Wang[a,*], Ming Zhang[a], Yangyang Fang[a], Yu An[a], Yingqi Chen[a], Liyan Dai[a,*]

[a] College of Chemical and Biological Engineering, Zhejiang University, Zhejiang Provincial Key Laboratory of Advanced Chemical Engineering Manufacture Technology, Hangzhou, 310027, PR China
[b] Institute for Micro Process Engineering (IMVT). Karlsruhe Institute of Technology (KIT), Hermann-von-Helmholtz-Platz 1, Eggenstein-Leopoldshafen, 76344, Germany

ARTICLE INFO

Keywords:
Alcohol oxidation
Synergic catalysis
Zn-W oxides
Heterogeneous catalysis

ABSTRACT

Bifunctional catalysts have been considered to have vital importance in catalytic chemical process, but there is still some developing room for convenient materials with dual active sites. These catalysts have a notorious reputation for inhibiting mutual neutralization and controlling the distribution of active sites in order to perform their functions. We tailor a series of W-*Zn*-Al_2O_3 catalysts by modulating the doping density of metal species, which can boost the catalytic process of alcohols into corresponding carbonyl compounds in an additive-free-condition. Test results indicate that the proper content of zinc element can promote the overall activities, and subsequent adjustment of doping zinc can dramatically increase the electronic interaction and change the distribution of chemical active sites. Also, a plausible reaction mechanism was proposed to better understand the acid-base bifunctional catalytic process. Theoretical results confirm this system can provide certain references for similar reactants. Present reaction system is a green procedure and features a broad substrate scope, which reveals a sustainable method to process oxidative dehydrogenation reaction.

1. Introduction

Recently, efficient and sustainable chemoselective dehydrogenation for alcohols has attracted extensive attentions, considering the environment issues[1] Numerous heterogeneous noble metal-based catalysts (*e.g.*, Au [2], Ag[3], Ru [4] and Pd[5]) as well as some non-noble transitional metal catalysts (*e.g.*, Cu[6], Co [7], Ni [8], Fe [9] and Mn [10]) have been developed recently to generate the selective oxidation reaction of aryl or alkyl alcohols. But high costs, scarcity of noble metal, the limited efficiency of non-noble catalyst and harsh reaction conditions to some extent confine their application in the chemical industry. To date, bifunctional catalysts have sparked increasing attention and have been widely applied in organic reactions [11] or used as an electrocatalyst [12] due to their acid-base properties and higher catalytic activities [13]. For instance, C. Hammond et al. compared the catalytic conversion in a bifunctional system with a monofunctional catalytic system. The bifunctional catalytic system exhibited more selective and higher catalytic performance and obtained (butoxy) methyl furan in an excellent yield.[13][b] With regard to safety and cost-efficiency, bifunctional catalyst, broadly feasible in organic synthesis, has been recognized as a promising candidate for the production of aldehydes [14]. Traditionally, this chemical transformation uses corrosive or toxic oxidants to facilitate the reaction, which violates the purpose of green chemistry [15]. Through the lens of green process, "soft" oxidants (*e.g.,* O_2 and H_2O_2) appear to be better choices to conduct this catalytic transformation, which can minimize toxic pollutants and wastes [16]. So, using cleaner oxidants combined with cheaper and environmental-friendly bifunctional catalysts to conduct the dehydrogenation reaction efficiently under mild conditions were highly appreciated.

Considering the synergetic effect between supports and immobilized metal species on dehydration performance, much more attention has been brought to synthesize supported bifunctional catalysts [17]. For example, Y. Iwasawa et al. selected organic amine functional group to modify silica/alumina oxides surface and created an acid-base catalyst, which was capable of accelerating the C—C coupling process []. Although, the coexistence of acid-base sites has made diverse bifunctional catalysts, catalysts decorated with dual active sites do face some challenges, such as the cross-intersection of acid/base sites and uneven distribution of the dual centers, which hindered the practical application [18].

Attempts have been made to tackle these obstacles. As regards an

* Corresponding authors.
E-mail addresses: wangxiaozhong@zju.edu.cn (X. Wang), dailiyan@zju.edu.cn (L. Dai).

https://doi.org/10.1016/j.mcat.2020.111114
Received 12 May 2020; Received in revised form 22 June 2020; Accepted 6 July 2020

efficient and a green preparation method, using polymeric aggregates to encapsulate acidic and basic group or incorporating acidic and basic groups over metal-organic framework is also a practical method to prepare bifunctional catalysts.[19] For example, a core-shell structured catalyst was synthesized by WG. Song et al. The inner core (Mg-Al mixed oxides) served as basic sites, and Al-containing mesoporous silica acted as an outer shell to provide acid sites. Due to the well-dispersion of active sites in prepared catalyst, this catalytic system performed well in Knoevenagel condensation reaction []. However, the preparation processes were generally complex and lengthy. In addition, they could result in uncertainty of catalytic activity, which caused high operation cost and large amount of energy consumption [20]. Thus, a straightforward preparation method of acid-base bifunctional catalysts is highly desirable. It is also of great necessity to select a suitable support for the high dispersion and the incorporation of the active sites [,21]

Herein, we successfully tailored W/Zn-Al_2O_3 bifunctional catalysts in a straightforward synthesis method by means of changing the introducing amount of zinc species. Benefiting from the coexistence of active sites in 15W-2.3Zn-Al_2O_3 and the promotional synergistic effect, the oxidative dehydrogenation reaction proceeded efficiently of aryl or alkyl alcohols without the need for additives. The catalyst can be easily regenerated without significant activity loss. Moreover, it is an interesting discovery that introducing a certain amount of metal species can adjust the acid − base property over catalyst surface as well as control the distribution of chemical active sites, thereby accelerating the oxidative dehydrogenation reaction under mild conditions.

2. Experimental section

2.1. Materials

Solvents and substrates used in reaction were purchased from Sinopharm Chemical Reagent Co., Ltd and Aladdin without further purification. Zinc acetate dehydrate ($Zn(CH_3COO)_2{\cdot}2H_2O$), ammonium tungstate ($H_{40}N_{10}O_{41}W_{12}{\cdot}xH_2O$), Al_2O_3 (99.99 % metals basis, powder) and H_2O_2 aqueous solution (30 wt%) were commercially available.

2.2. Catalyst preparation

The W − Zn − Al_2O_3 catalysts were prepared according to the following process. Taking the preparation of 15W − 2.3Zn − Al_2O_3 as an illustration, $Zn(CH_3COO)_2{\cdot}2H_2O$ (170 mg) as the source for zinc was dissolved in 100 mL deionized water containing Al_2O_3 (2.0 g). After vigorous stirring for 1 h, the slurry was evaporated to remove the water and then calcined in a muffle oven at 300 °C for 2 h to obtain Zn − doped Al_2O_3. Afterwards, 60 mL of $H_{40}N_{10}O_{41}W_{12}{\cdot}xH_2O$ (276 mg) aqueous solution containing Zn − doped Al_2O_3 (1.0 g) was also treated under vigorous stirring for 4 h. The solution was aged for 20 h, followed by evaporating excess water at about 70 °C under continuous stirring. The resulting solid was ground into fine powder and then treated by air calcination at 400 °C for 3 h to give the catalyst. For convenience, the calcined samples were labelled as xW − yZn − Al_2O_3, (x, y represent mass percentage of W, Zn, metal base). For comparison, monometallic oxide catalysts with Al_2O_3 as support were prepared with the same method above using the referring metal precursors, and nominated as W − Al_2O_3 and Zn − Al_2O_3 respectively.

2.3. General

X − ray diffraction (XRD) spectra were recorded on a PANalytical X' Pert diffractometer (Almelo, Netherlands) employing a Cu Kα radiation (λ = 1.5406 Å). Transmission electron microscopy (TEM) and high − resolution TEM (HRTEM) measurements were conducted to observe the morphology of the catalyst on a FEI Tecnai G^2 F20, operating at 200 kV. Prior to the test, the samples were ground to powder and ultrasonic dissolved into anhydrous ethanol, followed by dropping the dispersion onto a carbon − coated copper (Cu) grid. Field emission scanning microscopy (FESEM) images were collected on a Hitachi SU − 70 microscope combined with energy dispersive X − ray spectrometer (EDS) conducted on X − Max^N 80 T, Oxford Instruments, UK. FT − IR spectra of samples were obtained on an IRAffinity − 1S (Shimadzu, Japan) spectrometer using KBr pellets in a range of 400 − 4000 cm^{-1}. X − ray photoelectron spectroscopy (XPS) was performed on a Thermo Scientific Escalab 250Xi spectrometer using monochromatic Al Kα radiation (1486.6 eV), and the obtained XPS data was calibrated according to the reference C 1s peak at 284.8 eV. The nitrogen adsorption − desorption test was performed at −196 °C with a Micromeritics ASAP 2460 Version 2.01 to get the textual properties of samples. Prior to the tests, all samples were outgassed at 200 °C for 3 h. The surface area of each catalyst was obtained using the Brunauer, Emmett and Teller (BET) method. The pore volumes and pore diameters were calculated by the BJH method, respectively. Inductively coupled plasma (ICP) emission was used to analyze the content of metal ions of prepared samples and detect the leaching of metal species in reaction (ICP–OES, Optima 2100DV). To quantify the concentration and strength of acid and base sites, the heat of adsorption of NH_3 and CO_2 were carried out using an AutoChemII 2920 (Micromeritics, USA).

2.4. Activity tests

The catalytic oxidation of benzyl alcohol was conducted in a sealed regular glass reactor at 80 °C under magnetic stirring. Typically, 1.0 mmol of benzyl alcohol, 16 mg of catalyst and 1 mL of solvent were added into the reactor. While stirring, 1.7 mmol of hydrogen peroxide (30 wt% aq. solution) was added into mixture solvent, then increasing temperature up to 80 °C to start the reaction. After completion of the oxidative reaction, collecting the solid catalyst by centrifugation when the system cooled to room temperature. The products were identified by comparing their retention time with standard substances by a gas chromatograph (Agilent 6820, flame ionization detector, 30 m OV − 1701 capillary column) and reconfirmed by GC − MS (Agilent 6890 − 5973). In order to assure the reproducibility, the content analysis of products was calculated with an external standard method at least three times.

3. Results and discussion

3.1. Catalyst characterization

X − ray diffraction (XRD) patterns of Zn − Al_2O_3, 15W − Al_2O_3 and a series of W/Zn Al_2O_3 catalysts were investigated as shown in Fig. 1. Al_2O_3 exhibited (012), (104), (110), (113) and (116) characteristic peaks in all samples (JCPDS No. 10 − 0173). As regards Zn − Al_2O_3, the peaks located at 2θ = 31.77°, 34.42°, 36.25°, 47.54° and 56.60° can be ascribed to (100), (002), (101), (102) and (110) planes of hexagonal ZnO phase (JCPDS NO. 36 − 1451), respectively [22]. In 15W − Al_2O_3 catalyst, the strong peaks appeared at 2θ = 23.08°, 23.71°, 24.10°, 28.77° and 34.02°, corresponding to (001), (020), (200), (111) and (220) planes of the orthorhombic − phase WO_3 (JCPDS NO. 20 − 1324) [23]. Adding ZnO to Al_2O_3 leads to the intensity change of WO_3 from orthorhombic phase to low detection (Fig. 1a). As supported in Fig. 1b, the phase of $ZnWO_4$ peaks (JCPDS NO. 15 − 0774) was not observed clearly for samples with low zinc concentrations (2.3 wt%), indicating the mono − dispersion of W and Zn species might highly relied on the unbalanced content. FT − IR spectra show that there are no characteristic bands owning to dopant W metal, which are in good consistent with XRD results (Figure S1). With the addition of W and Zn species, the band at 628 cm^{-1} occurred, which can be related to the vibration of tetrahedral M − O bond. With an increase contents of Zn element, the half − peak breadth of the bands at 514 cm^{-1} get broader while intensity of the representing Al_2O_3 reduced. These results become compelling evidences that the dopants have certain interaction with

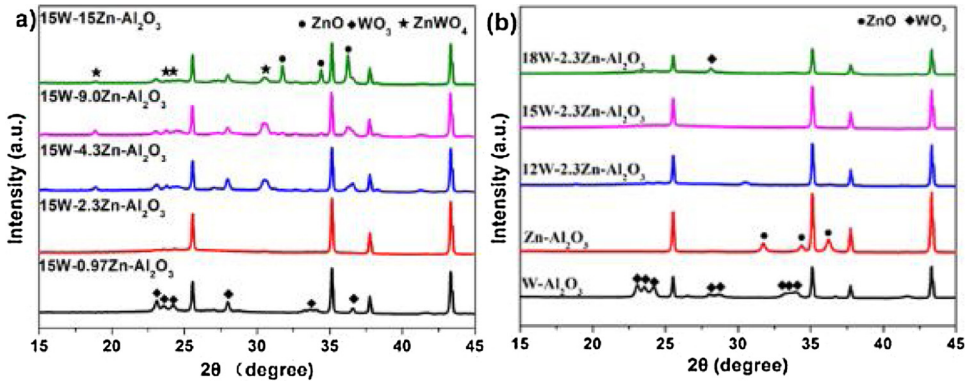

Fig. 1. XRD patterns of samples calcined at 400 °C.

Al_2O_3 or even incorporated into the structure of Al_2O_3 [24].

SEM and TEM measurements were used to investigate the morphology of the prepared W/Zn − Al_2O_3 catalysts. The resulting images indicated that the morphological structure could be controlled and tuned by introducing different amount of metal dopants. Tungsten shows as an oxide and successfully loads on the support surface rather than into the structure of Al_2O_3 if the zinc element is insufficient (Fig. 2a). It can be seen in Fig. 2c that some square nanostructures (the yellow rectangle represents WO_3) are loaded on the support when the introduction amount of zinc element is about 4.3 wt%. When the content ratio of W and Zn is 1:1, ZnO phase became clearly as regards the aggregation of Zn species (Fig. 2d). Interestingly, no W or Zn oxides are found when the introduction amount of zinc element is about 2.3 wt%, which is also a favorable evidence of increasing interaction between dopant ions and support (Fig. 2b). The W, Zn, Al, and O elements distribution of prepared catalyst were characterized by the elemental mapping (Fig. 2e) and the EDS results in Figure S2a verified the relatively homogeneous distributions of those elements. Fig. 2f-h shown the TEM, STEM and HRTEM images of the 15W − 2.3Zn − Al_2O_3 catalyst. The lattice spacing of obtained sample was calculated from high − resolution TEM (Fig. 2h, Fig. S2b), however, the interface between W, Zn and the support matrix could not be identified clearly, indicating the existence of the strong metal − support interactions.[14]^{b} HAADF − STEM was employed to investigate the internal structure, Fig. 2g shown the whole morphology feature of 15W − 2.3Zn − Al_2O_3 and no WO_3 or ZnO species were presented of the surface. It surprised us that some metal oxides particles were clearly occurred at the thinner edges of the Al_2O_3 support, indicating W and Zn species were surly incorporate into the structure of Al_2O_3 [25].

.XPS was further used to analyze the elemental composition and

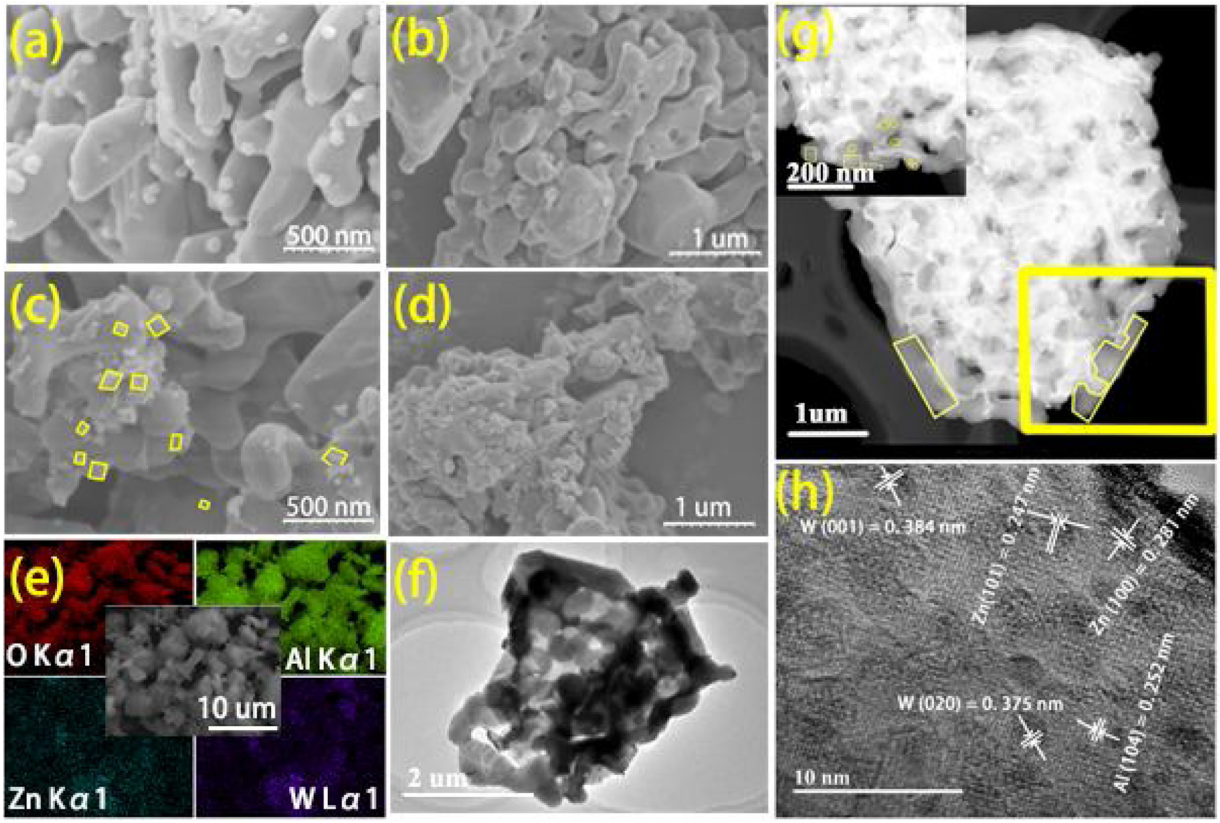

Fig. 2. FESEM images of (a) 15W − 0.97Zn − Al_2O_3, (b) 15W − 2.3Zn − Al_2O_3, (c) 15W − 4.3Zn − Al_2O_3, (d) 15W − 15Zn − Al_2O_3, (e) the corresponding elemental distribution mapping of 15W − 2.3Zn − Al_2O_3. TEM (f), STEM (g) and HRTEM (h) images of 15W − 2.3Zn − Al_2O_3 sample. The inset in (g) displayed a marked area.

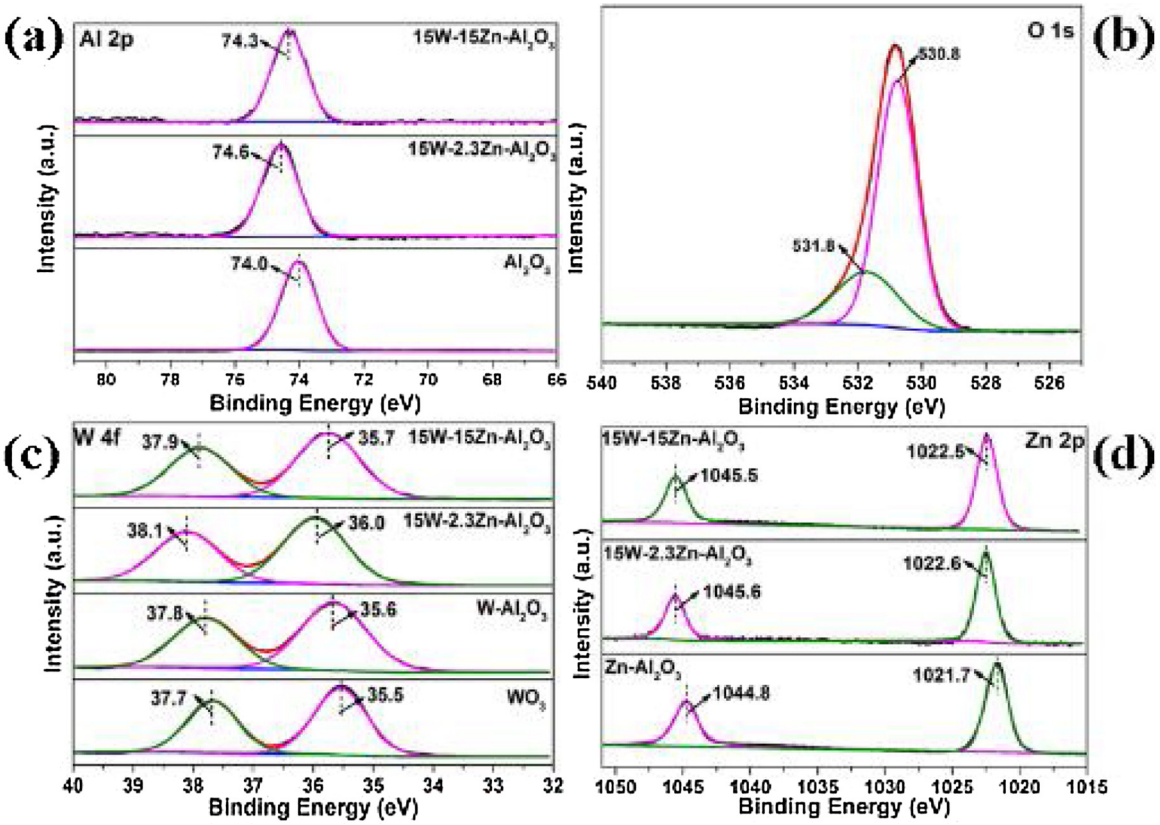

Fig. 3. High resolution XPS spectrum of (a) Al 2p of pure Al_2O_3, 15W − 2.3Zn − Al_2O_3 and 15W − 15Zn − Al_2O_3, (b) O 1s of 15W − 2.3Zn − Al_2O_3, (c) W 4f spectra of WO_3, 15W − Al_2O_3 and 15W − 2.3Zn − Al_2O_3, (d) Zn 2p spectra of Zn − Al_2O_3 and 15W − 2.3Zn − Al_2O_3.

chemical state of the obtained samples. The wide − range XPS spectrum in Fig. S3 clearly demonstrates the presence of Al, O, W and Zn elements in the 15W − 2.3Zn − Al_2O_3 catalyst, which is well consistent with the EDS results. Fig. 3a shows the binding value at 70.4, 74.6 and 74.3 eV assigned to Al 2p doublets for pure Al_2O_3, 15W − 2.3Zn − Al_2O_3, and 15W − 15Zn − Al_2O_3, respectively [26]. The O 1s spectrum can be divided into two peaks, as shown in Fig. 3b, one peak can be indexed as the O − W bond (530.8 eV) and the other at 531.8 eV is corresponding to the hydroxyl groups (−OH) over the obtained sample surface, respectively [27]. Pristine WO_3 was obtained *via* direct pyrolysis of $H_{40}N_{10}O_{41}W_{12}{\cdot}xH_2O$. The spectra of W 4f in Fig. 3c, as for WO_3 and 15W − Al_2O_3, two distinct characteristic peaks at 35.5 and 37.5 eV are respectively corresponding to W 4f7/2 and W 4f5/2 doublets, indicating the presence of W^{6+} in those prepared samples [28]. Notably, the binding energy values of W 4f doublets in 15W − 2.3Zn − Al_2O_3 are obviously larger than 15W − Al_2O_3 when introducing Zn species, and two peaks assigned to the W − Al bond and WO_3 move to higher binding energy (36.0 and 38.1 eV). This is a great consequence to verify the interaction between WO_3 and Al_2O_3, such as connected by the W − Al bond [29]. The bands at 1021.7 and 1044.8 eV are characterized to Zn 2p3/2 and Zn 2p1/2 respectively (Fig. 3d), and the binding energy of Zn 2p in 15W − 2.3Zn − Al_2O_3 both shift to higher position [22]. These phenomena may be attributed to the formation of the Al − O−M bonds in the crystal lattice, causing the change of the electron binding force and then the shift of the electron binding energy [30]. Furthermore, the surface proportions of W and Zn in 15W − 2.3Zn − Al_2O_3 are further detected by XPS with the calculated contents of 5.8 % and 2.37 %, respectively. The decrease content of W element demonstrates the formation of the strong W − Al interactions or dopant tungsten is precisely penetrated into the Al_2O_3 lattice as well [,25]. Overall, the binding energy shift of various zinc loading samples indicated a strong metal − support interaction and revealed the possibility of electronic interaction modulation [].

The N_2 adsorption − desorption isotherms and pore size distributions of pure Al_2O_3, 15W − Al_2O_3, 15W − 2.3Zn − Al_2O_3 and 15W − 15Zn − Al_2O_3 were depicted in Fig. S4, to investigate zinc doping influence of the textural parameters. The occurrence of the typical type V isotherm with a H3 hysteresis loop can be found in each sample [31]. As listed in Table S1, all samples shown the low surface area and the small pore value. Though, the low specific surface area of the prepared samples might be ascribed to the limited number of pores, it was reasonable to assume prepared materials were non-porous.

The temperature − programmed desorption of NH_3 and CO_2 have been extensively used to test the acid − base properties over the catalysts surface, in order to verify the improved catalytic activity with doping W/Zn species on Al_2O_3 and modulation of the acid − base sites [32]. Broad desorption peaks can be observed for either CO_2 or NH_3 profiles, which can be deconvoluted to three peaks based on the desorption temperature. As shown in Fig. 4, three desorption peaks in CO_2 − profile can be identified as the weak site (150 − 220 °C), moderate site (220 − 350 °C) and strong base site (above 350 °C), respectively [22,33]. NH_3 − TPD profiles are also deconvoluted to three peaks with maximal temperature in the region of 110 − 135 °C, 220 − 260 °C, 330 − 400 °C, corresponding to weak, moderate and strong acid sites, respectively [].

In general, the amount of desorbed NH_3/CO_2 represented the concentration of the acid/base sites. It was observed that the dominant sites in 15W − 2.3Zn − Al_2O_3 (400) were the weak acid/base sites and the strong acid/base sites. Furthermore, the type of dominant acid − base sites changed obviously due to the mutual neutralization with the addition of Zn as well as the occurrence of new phases at higher calcination temperature. Specifically, increasing zinc loading can reduce the strong acid sites, and the high calcination temperature can eliminate the strong base/acid sites but maintaining the moderate

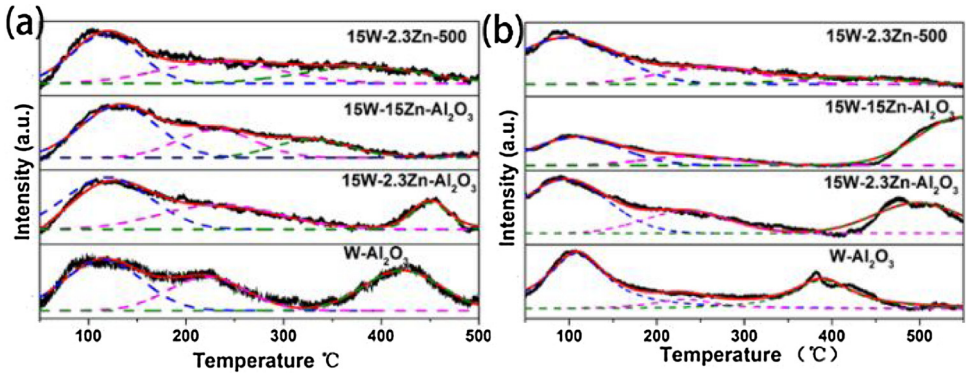

Fig. 4. (a) NH_3-TPD and (b) CO_2-TPD profile of $15W-Al_2O_3$, $15W-2.3Zn-Al_2O_3$, $15W-15Zn-Al_2O_3$ and $15W-2.3Zn-500$ ($15W-2.3Zn-Al_2O_3$ calcined at 500 °C), respectively.

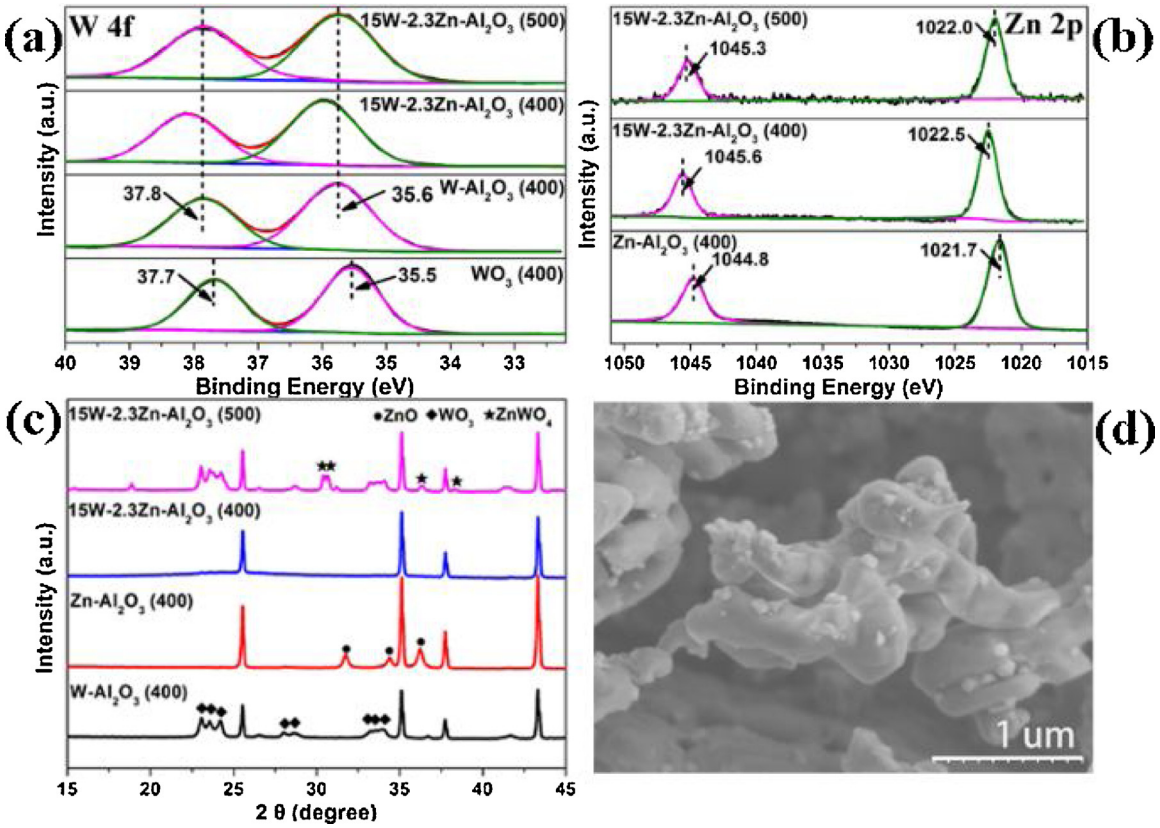

Fig. 5. High resolution XPS spectrum of (a) W 4f spectra of WO_3, $15W-Al_2O_3$, $15W-2.3Zn-Al_2O_3$ (400) and $15W-2.3Zn-Al_2O_3$ (500). (b) Zn 2p spectra of $Zn-Al_2O_3$, $15W-2.3Zn-Al_2O_3$ calcined at 400 °C and 500 °C, respectively. (c) XRD patterns of $15W-2.3Zn-Al_2O_3$ (400) and $15W-2.3Zn-Al_2O_3$ (500). (d) FESEM image of $15W-2.3Zn-Al_2O_3$ calcined at 500 °C.

and weak sites. According to the literatures,[34] low − coordinated oxygen anions may account for the strong basic sites in catalysts, which can be supported by XPS analysis. Because ZnO_x ubiquitously used as amphoteric oxides and WO_3 possessed the strong Lewis acidity,[35] the O^{2-} surrounded on the Zn^{2+} might be a reason for the occurrence of basic sites.[36] The occurrence of WO_3 and $ZnWO_4$ phases in $15W-2.3Zn-Al_2O_3$ (500), as detected by XRD (Fig. 5c), might promoted the mutual neutralization of acid/base sites, weakening the intensity of strong acid and base sites.

3.2. Catalytic Activity of the prepared catalysts

Herein, the oxidation of benzyl alcohol in the absence of additives was used as a probe reaction to give intuitive observation into the synergistic effect of prepared metal − doped catalysts and their acid − base properties. As listed in the Table 1, $15W-2.3Zn-Al_2O_3$ catalyst exhibits excellent conversion (97.5 %) and selectivity (95.2 %) for this chemical transformation (Table 1, Entry 4). Compared with $15W-2.3Zn-Al_2O_3$, $Zn-Al_2O_3$ catalysts with different amount of W can also catalyze the reaction but with lower conversion or selectivity (Table 1, Entry 8, 9). To better exhibit the effect of W content in catalytic performance, we also have carried out the reaction using varied mass percentage of $W-Al_2O_3$ catalysts (Table 1, Entry 11–15). With the increasing tungsten amount, the conversion increased first and then decreased steadily. In short, the catalytic performance of monometallic oxide catalysts was inferior than bi-component catalyst and the doping of zinc could enhance the whole catalytic activity. The catalytic activity is unsatisfactory in the absence of the catalyst (Table 1, Entry 16) and the yield of desired product was only 13.5 %. Upon the increase of catalyst amount (16 mg), both the conversion of benzyl alcohol and the

Table 1
Catalytic performance of prepared catalysts[a].

Entry	Catalyst	Conv. (%)	Sel. (%)	Yield (%)
1	15W-Al_2O_3	60.6	99.9	60.5
2	2.3Zn-Al_2O_3	11.8	99.9	11.8
3	15W-0.97Zn-Al_2O_3	99.2	89.5	88.8
4	15W-2.3Zn-Al_2O_3	97.5	95.2	92.9
5	15W-4.3Zn-Al_2O_3	88.6	76.7	68.0
6	15W-9.0Zn-Al_2O_3	76.6	99.9	76.5
7	15W-15Zn-Al_2O_3	33.4	78.0	26.1
8	12W-2.3Zn-Al_2O_3	94.3	96.5	91.0
9	18W-2.3Zn-Al_2O_3	27.5	99.9	27.5
10	15W-2.3Zn-Al_2O_3[b]	64.2	89.3	57.3
11	5W-Al_2O_3	38.2	99.9	38.2
12	10W-Al_2O_3	58.5	91.5	53.5
13	12W-Al_2O_3	63.8	95.5	60.9
14	18W-Al_2O_3	55.8	99.9	55.7
15	25W-Al_2O_3	52.4	99.9	52.3
16	None	13.5	100	13.5

[a] Reaction conditions: benzyl alcohol (1.0 mmol), H_2O_2 (1.7 mmol), CH_3CN (1 mL), 16 mg of catalyst, 80 °C, 6 h.
[b] The catalyst was calcined at 500 °C.

selectivity of benzaldehyde have no significant increase (Fig. S5).

Furthermore, we compared current catalytic system with other catalytic system for the selective oxidation of benzyl alcohol, and the data was presented in Table 2. The data clearly verified that present catalyst had remarkable catalytic activities in oxidative dehydrogenation reaction in an additive-free-condition.

Moreover, we calculated the turnover frequency (TOF) of some typical catalysts in the present system from the first 20 min.. The TOF value of 15W − 2.3Zn − Al_2O_3 (42.2 h^{-1}) was distinctly larger than that of other catalysts, which was consistent with the catalytic performances (Table 3). The aggregation of active species on the surface of 15W−15Zn − Al_2O_3 may account for such a low TOF value under identical reaction system. Attention should be paid that when 15W − 2.3Zn − Al_2O_3 sample was calcined at 500 °C, the catalytic activity decreased dramatically and the yield of target product was 1.6 times smaller than using the catalyst calcined at 400 °C (Table 1, Entry 10). As regards, XRD, SEM, XPS, NH_3−TPD and CO_2−TPD measurements were used to explore structural difference and neutralization in these two catalysts. Interestingly, the binding energy values of W and Zn doublets were obviously shift to lower position compared with the low − temperature calcined sample (Fig. 5a, 5b). The values of W doublets in 15W − 2.3Zn − Al_2O_3 (500) were almost same as 15W − Al_2O_3 (400), indicating that the formation of strong W − Al bond highly depended on the calcination temperature and the participation of dopant ions. Because W and Zn elements have the tendency to sinter into larger species during high temperature calcination temperature, some active metal have aggregated over the support surface in 15W − 2.3Zn − Al_2O_3 (500), leading to the difference morphology of the 15W − 2.3Zn − Al_2O_3 (500) and 15W − 2.3Zn − Al_2O_3 (400) (Fig. 5d). Furthermore, the content ratio of W, Zn is increased to 3.60 over the 15W − 2.3Zn − Al_2O_3 surface when it is calcined at 500 °C,

Table 3
Catalytic activity of prepared catalyst[a].

Catalyst	Conv. (%)	Sel. (%)	TOF (h^{-1})
15W-Al_2O_3	11.3	99.9	26.0
2.3Zn-Al_2O_3	3.9	99.9	20.7
15W-2.3Zn-Al_2O_3	26.3	99.9	42.2
15W-15Zn-Al_2O_3	5.5	99.9	3.3
15W-2.3Zn-Al_2O_3[b]	5.6	99.9	9.0

[a] Reaction conditions: benzyl alcohol (1.0 mmol), H_2O_2 (1.7 mmol), CH_3CN (1 mL), 16 mg of catalyst, 80 °C, 1/3 h.
[b] The catalyst was calcined at 500 °C.

almost 1.5 times larger than sample calcined at 400 °C. Additionally, the profiles in NH_3−TPD and CO_2−TPD (Fig. 4) indicating that bifunctional property has an important contribution of dehydrogenation activity. The sample with same concentration of the W and Zn species but calcined at 500 °C, displayed inferior catalytic activity due to the aggregation of active sites, if not, the unbalanced distribution of acid and base sites over the support surface, compared to the sample calcined at 400 °C.

Moreover, some experiments were conducted using 15W − 2.3Zn − Al_2O_3 as the representative catalyst over different reaction parameters, such as solvent nature, oxidant dosage, reaction temperature and reaction time, to investigate the catalytic activity in detail. The solvent effect is very important for the selective oxidation performance. Fig. 6a exhibited that the conversion of benzyl alcohol was poor when using ethyl acetate as a solvent, which might be account for the poor miscibility of oxidant and the low reaction temperature. In addition, tetrahydrofuran or methanol was not suitable for this chemical transformation. The selectivity of benzaldehyde was excellent when using CH_3CN as a solvent, which might be due to the suppression of the formation of other by − products by its property, and good solubility for the reactant and product as well [37]. Notably, hydrogen peroxide alone is regarded as a poor oxidant in reaction and usually needs to be activated by a catalyst so that efficiently perform the oxidation. Nitriles have been employed as an accelerant for this activation as reported [38]. Deming, PH et al. came up with ideas that hydrogen peroxide in combination with acetonitrile (CH_3CN) as the solvent generated a reactive intermediate (peroxyimidic acid), which could also act as an effective oxidant for various reactions []. Some experiments were performed to verify the terminal oxidant (H_2O_2 or peroxyimidic acid) in our catalytic system (Fig. 6b). We compared the catalytic performance of our reaction system in the following three solvents in detail: acetonitrile, ethyl cyanoacetate and N,N − Dimethylformamide, finding the results in the order acetonitrile > N,N − Dimethylformamide > ethyl cyanoacetate. If hydrogen peroxide in our system is activated by the nitrile and then produce a peroxycarbonmidic acid, the yield of desired product in ethyl cyanoacetate will same as acetonitrile to some degree and the reaction performance will have no difference with and without the participation of catalyst. If the true oxidant is peroxyimidic acid, using N,N − Dimethylformamide as a solvent will have a negative effect in catalytic

Table 2
The comparison of catalytic performance of 15W − 2.3Zn − Al_2O_3 with other published data in benzyl alcohol oxidation.

Entry	Catalyst	Oxidant	Solvent	Reaction Conditions	Conv. (%)	Sel. (%)	Yield (%)	Ref.
1	15W-2.3Zn-Al_2O_3	H_2O_2	CH_3CN	80 °C, 6 h	97.5	95.2	92.9	Herein[a]
2	Ag/WO_3(PEG 4000)	None	Toluene	110 °C, 6 h, base	98	98	96.0	3a
3	Ru^0/γ-Al_2O_3	O_2	*tert*-amyl alcohol	9 bar, 160 °C, continuous flow	50	99.9	50.0	4b
4	Pd-STO	O_2	*n*-hexane	69 °C, 24 h, K_2CO_3	> 99	> 99	> 99	5a
5	$CuCl_2$@MOF-NH_2	Air	CH_3CN	70 °C, 6 h	> 99	> 99	> 99	6c
6	Pd/CoMagSBA	O_2	None	90 °C, 6 h	70.0	77.0	53.9	7
7	$Fe(NO_3)_3{\cdot}9H_2O$, TEMPO	Air	Toluene	100 °C, 1 h, KOH	> 99	> 99	> 99	9
8	MnP-AMP (S_{345})	Air	CH_3CN	40 °C, 2 h, isobutyraldehyde	100	98	98	10

[a] Reaction conditions: benzyl alcohol (1.0 mmol), H_2O_2 (1.7 mmol), CH_3CN (1 mL), 16 mg of catalyst, 80 °C, 6 h.

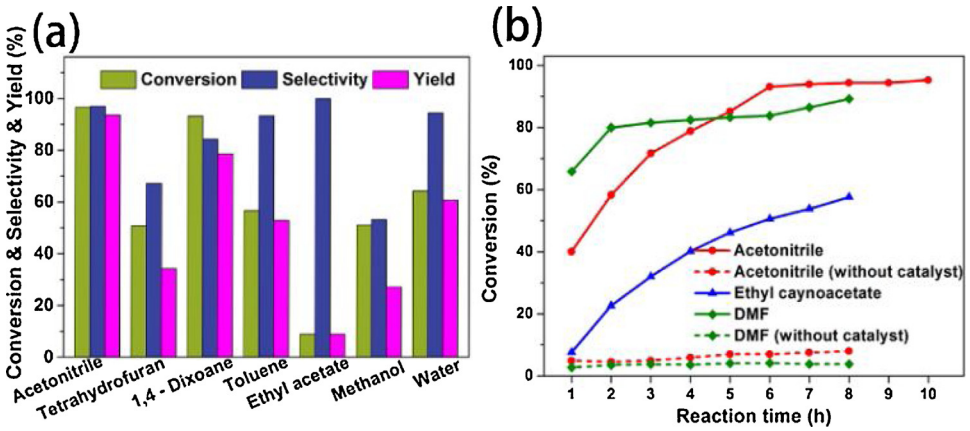

Fig. 6. (a) Effects of solvents nature, (b) deep insights of the reaction using hydrogen peroxide as an oxidant. Reaction conditions: benzyl alcohol (5.0 mmol), H_2O_2 (8.5 mmol), Solvent (5 mL), 80 °C, 6 h, 80 mg of 15W − 2.3Zn − Al_2O_3 catalyst or 0 mg.

performance. Because the amide could not react with H_2O_2 to give the peroxycarboximidic acid intermediate []. However, these are not the case, using DMF as a solvent also have a good conversion (Fig. 6b). Moreover, the conversion in the condition that using H_2O_2 as an oxidant, CH_3CN or DMF as a solvent but in the absence of the catalyst is poor, which may confirm that H_2O_2 in our system is activated by 15W − 2.3Zn − Al_2O_3 catalyst rather than the acetonitrile. Meanwhile, these results verify that 15W − 2.3Zn − Al_2O_3 have a good catalytic performance and can facilitate the reaction process well.

The influence of the oxidant dosage was also investigated, as presented in Fig. 7a. The conversion increased rapidly with increasing molar ratio of H_2O_2 to benzyl alcohol and then reached a steady stage. But the excess amount of oxidant, especially H_2O_2 to benzyl alcohol molar ratio reached 2:1, would decrease the selectivity of benzaldehyde significantly due to the further oxidation to form benzoic acid. The reaction temperature effect in this catalytic reaction was also investigated (Fig. S6). The conversion of reactant was obviously increased and the selectivity to benzaldehyde kept steady with the increasing reaction temperature, indicating this reaction might be sensitive to the change of the temperature and this reaction was endothermic. Reaction time was also an important factor needed to be studied, and we found that the conversion of reactant reached 93.1 % while proceeded for 6 h (Fig. 7b). Prolonging the reaction time, the conversion kept constant but had a tendency to form benzoic acid, resulting in the decrease of the selectivity.

3.3. General applicability

Encouraged by the favorable experiment results, we extended the reaction using different types of alcohols as the substrate over the 15W − 2.3Zn − Al_2O_3 catalyst to verify the general applicability of present catalytic system (Table 4). Interestingly, substrates were oxidized to the corresponding products with moderate to excellent yields regardless of substituents nature, the electron − donating or the electron − withdrawing groups [39]. The only by − product of those substrates was the corresponding acid, which was confirmed by GC − MS (Fig. S7). Analyzing the results more deeply, we found that electron − withdrawing groups have a slightly negative influence of the catalytic activity compared with electron − donating groups (Table 4, Entry 2 − 4). In the meantime, the dehydrogenation reaction of aliphatic alcohol (pentan − 2 − ol) was also proceed efficiently and gained

Table 4
Oxidation of various alcohols catalysed by 15W − 2.3Zn − Al_2O_3[a].

Entry	Substrate	Product	Conv. (%)	Sel. (%)
1			97.5	95.2
2			96.7	98.8
3	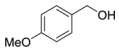	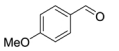	93.6	99.0
4	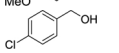	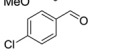	76.6	100
5			72.6	100
6			71.3	100
7			52.1	100

[a] Reaction conditions: substrate (1.0 mmol), H_2O_2 (1.7 mmol), CH_3CN (1 mL), 16 mg of 15W − 2.3Zn − Al_2O_3, 80 °C, 6 h.

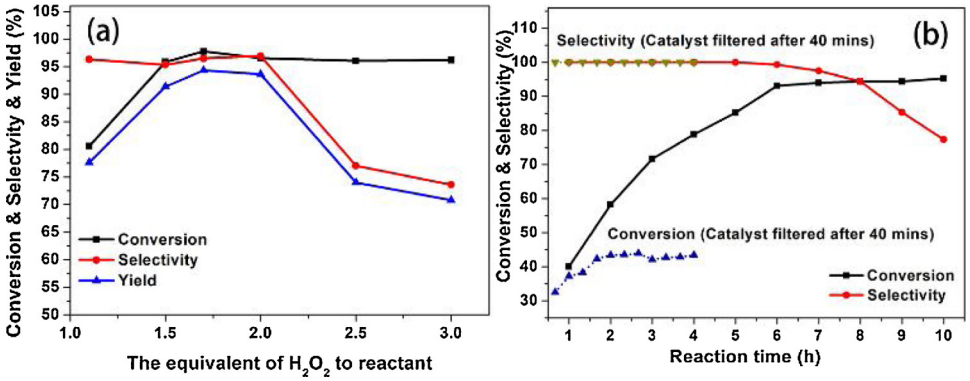

Fig. 7. Effects of (a) the molar ratios of H_2O_2 to reactant and (b) reaction time on catalytic performances over 15W − 2.3Zn − Al_2O_3 catalyst. Reaction conditions: benzyl alcohol (5.0 mmol), H_2O_2 (8.5 mmol), CH_3CN (5 mL), 80 mg of 15W − 2.3Zn − Al_2O_3 catalyst, 80 °C, 6 h.

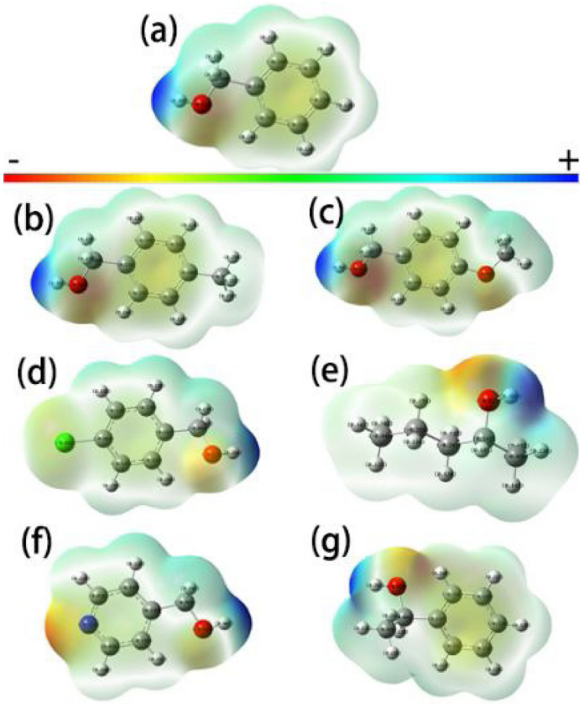

Fig. 8. Charge distribution and the electron density of the substrates calculated by Gaussian: (a) benzyl alcohol, (b) 4 − methyl benzyl alcohol, (c) 4 − methoxybenzyl alcohol, (d) 4 − chlorobenzyl alcohol, (e) pentan − 2 − ol, (f) 4 − pyridinemethanol and (g) α − methylbenzyl alcohol.

a moderate yield (Table 4, Entry 5). However, less efficient catalytic performance was found when using 4 − pyridinemethanol as a substrate (Table 4, Entry 6). In order to get a relationship of the substrate structure and their reaction activity, we investigated the charge distribution and the electron density of the substrates at the B3LYP/6 − 31 G level of theory, using the Gaussian 09, Revision D.01 [40], finding that the theoretical results were in accordance well with the experimental conclusions. Substituent groups influenced the electron density of both the oxygen and adjacent carbon on the alcohol hydroxyl group, and the reaction activity might rely on the charge density difference between the oxygen and adjacent carbon (Fig. 8). In particular, the excellent yield was occurred when the electron density and charge value of substrates was similar to benzyl alcohol, and the low charge density (the yellow area) of oxygen on the alcohol hydroxyl group tended to decreased the reaction activity. In general, present system is favorable for both aryl and alkyl alcohols oxidation reaction, and can provide certain references for similar reaction.

3.4. Proposed reaction mechanism

Based on the characterization of the prepared catalysts, we assume that the reaction is processed on the external surface of the 15W − 2.3Zn − Al_2O_3, and the reaction mechanism has been proposed to better understand how the acid-base sites affects the oxidative dehydrogenation reaction. As illustrated in Scheme 1. Firstly, the hydroxyl group (− OH) in benzyl alcohol structures is prone to adsorbed on 15W − 2.3Zn − $Al_2O_3$with the medium-strong acid-base sites, and the absorbed O—H bond cleaved to present as an alcoholate intermediate [41]. As referred above, H_2O_2 in our system is activated by 15W − 2.3Zn − Al_2O_3 catalyst rather than the acetonitrile, and the strong acid sites of 15W − 2.3Zn − Al_2O_3 can activate the H_2O_2 to give the active oxygen species [42]. Subsequently, the adsorbed reactant molecules react with neighboring reactive oxygen species to proceed the cleavage of α-C–H bond, and thus form the benzaldehyde.

Based on the literatures, the surface basicity of prepared catalysts is conductive to the proton transformation from the hydroxyl group and the acidic sites are crucial for the dehydration step [,43]. Moreover, the acid sites can prevent the further oxidation of the substrates []. According to the CO_2 − TPD and NH_3 − TPD, 15W − 2.3Zn − Al_2O_3 (400) possesses more acid and basic sites than 15W − 2.3Zn − Al_2O_3 (500), and the catalytic activity are extremely different. Additionally, electron density of the substrates can support the above assumption of the mechanism. Because when the value of $O^{\delta-} - H^{\delta+}$ group, or more specifically, the electronegativity of the O species in molecular, is smaller, the reactants tend to be inert to the catalyst surface, so the reaction is less active. Therefore, the comparable catalytic performance in present catalytic system may be related to the surface acid/base sites on the catalysts.

3.5. Catalyst reusability

The study about the nature of prepared catalysts was performed by using 15W − 2.3Zn − Al_2O_3 as the representative catalyst under the optimal reaction conditions. A hot filtration test was performed firstly, in which the catalyst was removed from the system after 40 min. of reaction, and the filtrate continued to react. As indicated in Fig. 7b, the conversion increased slightly without the participation of 15W − 2.3Zn − Al_2O_3 at the beginning and then no further grown up. The conversion change might due to the leaching of the metal species or the existence of the active oxygen species. When the reaction was completed, the catalyst could be recovered by a simple phase separation, then was washed thoroughly and followed by drying at 70 °C overnight for next use. It was worth mentioning that there was no significant loss of the catalytic activity after six consecutive runs (Fig. 9). The XRD spectra of the used catalyst after six runs was shown in Fig. S8, confirming that the structure and morphology of the reused catalyst were nearly unchanged. To ensure the validity of the research, ICP-OES (Optima 2100DV) was further performed to calculate the ratio of the zinc and tungsten ions after each run in the reusability experiment (Table S2). The Zn/W ratio slightly increased to 0.1605 after 3 cycles, leading to a little decrease of the benzyl alcohol conversion in the fourth cycle. This phenomenon indicated that the tungsten species in prepared catalyst had a slightly leaching tendency after a few times of reuse but could maintain a good catalytic performance. Generally, 15W − 2.3Zn − Al_2O_3 had a good recyclability and exhibited excellent catalytic performance, which highlighted the application potential for oxidative dehydrogenation without additives in a future industrial scale.

4. Conclusion

In summary, an efficient and sustainable catalytic oxidation system of various alcohols without additions was proposed. Zn-doped bimetallic W − Zn − Al_2O_3 catalysts were prepared *via* an eco-friendly method. Controlling the amount of zinc will prevent the active metal from aggregation so that the resulting catalyst can exhibit significantly enhanced catalytic activity. 15W − 2.3Zn − Al_2O_3 catalyst, exhibited the highest catalytic activity, remarkable stability and is a potential candidate for selective catalytic oxidation of alcohols. Based on the characterization, XPS verified an interesting coordinating phenomenon between dopant ions and support. TPD measurement indicated that the acid − base property over the catalyst surface was sensitive to the catalytic performances, which could be modulated by changing the doping density of metal species. Moreover, the oxidation of a wide substrate scope without additions is a feature of present catalytic system. Therefore, the present work presents a sustainable process for obtaining carbonyl compounds by dehydrogenation reaction since it demonstrates a simple and environmental-friendly method for eliminating mutual neutralization and controlling the distribution of chemical active sites over bifunctional catalyst.

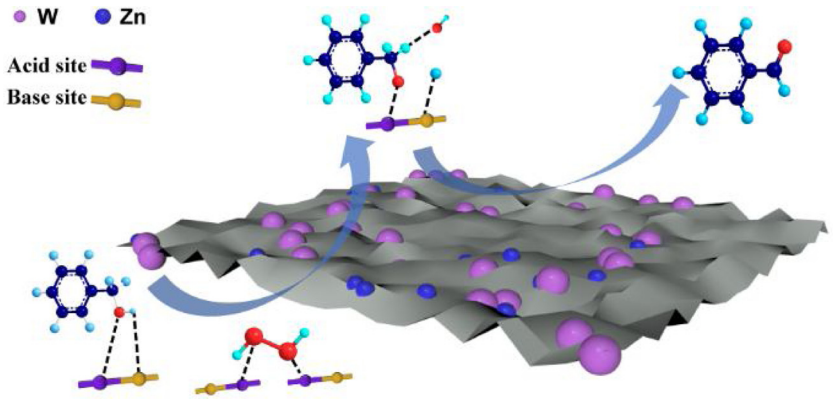

Scheme 1. Possible reaction mechanism for the oxidative dehydrogenation reaction over the 15W − 2.3Zn − Al_2O_3 catalyst.

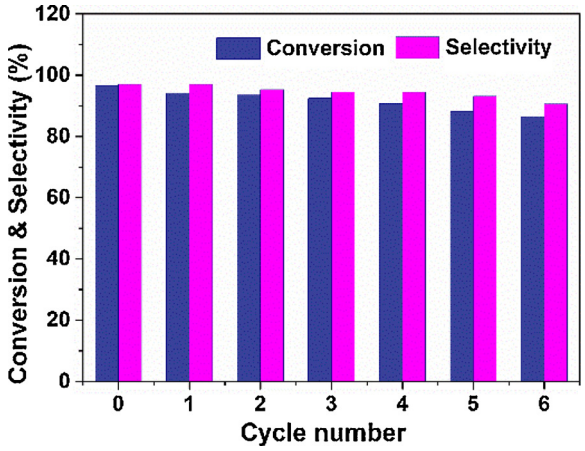

Fig. 9. Recycling experiments of the 15W − 2.3Zn − Al_2O_3 catalyst in the oxidative dehydrogenation of benzyl alcohol to benzaldehyde. Reaction conditions: benzyl alcohol (1.0 mmol), H_2O_2 (1.7 mmol), CH_3CN (1 mL), 16 mg of catalyst, 80 °C, 6 h.

Declaration of Competing Interest

The authors declare that we have no known competing financial interests or personal relationships that could have appeared to influence the work reported in this paper.

CRediT authorship contribution statement

Menglu Cai: Investigation, Formal analysis, Writing - original draft. **Jun Li:** Data curation, Writing - review & editing. **Xiaozhong Wang:** Visualization, Methodology, Resources. **Ming Zhang:** Writing - review & editing. **Yangyang Fang:** Writing - review & editing. **Yu An:** Writing - review & editing. **Yingqi Chen:** Resources, Writing - review & editing. **Liyan Dai:** Supervision, Resources, Writing - review & editing.

Acknowledgments

This work was supported by Zhejiang Provincial Key Laboratory of Advanced Chemical Engineering Manufacture Technology (No. 2017E10001), Zhejiang Province (China).

Appendix A. Supplementary data

Supplementary material related to this article can be found, in the online version, at doi:https://doi.org/10.1016/j.mcat.2020.111114.

References

[1] (a) A. Corma, S. Iborra, A. Velty, Chem. Rev. 107 (2007) 2411–2502;
(b) T.G. Brink, I.W.C.E. Arends, R.A. Sheldon, Science 287 (2000) 1636–1639;
(c) J.J. Wang, L. Tang, G.M. Zeng, Y.N. Liu, Y.Y. Zhou, Y.C. Deng, J.J. Wang, B. Peng, ACS Sustainable Chem. Eng. 5 (2017) 1062–1072.
[2] (a) A.J. Shakir, M. Florea, D.C. Culita, G. Ionita, C. Ghica, C. Stavarache, A. Hanganu, P. Ionita, J Porous Mater. 23 (2016) 247–254;
(b) H. Tsunoyama, H. Sakurai, Y. Negishi, T. Tsukuda, J. Am. Chem. Soc., React. Chem. Eng 127 (2005) 9374–9375.
[3] (a) P. Bappi, S. Sachin, D.P. Debraj, S.D. Siddhartha, B. Rajaram, Catal. Commun. 132 (2019) 105804–115808;
(b) T. Mitsudome, Y. Mikami, H. Funai, T. Mizugaki, K. Jitukawa, K. Kaneda, Angew. Chem. Int. Ed. 47 (2008) 138–141;
(c) K. Shimizu, K. Sugino, K. Sawabe, A. Satsuma, Chem. Eur. J. 15 (2009) 2341–2351.
[4] (a) J.P. Zhao, W.Y. Hermandez, W.J. Zhou, Y. Yang, E.I. Vovk, M. Capron, V. Ordomsky, ChemCatChem. 12 (2019) 238–247;
(b) J.S. Kreutzer, L. Vanoye, B. Guicheret, R. Philippe, E. Metay, M.C. Duclos, M. Lemaire, C. De Bellefon, P. Fongarland, A. Favre-Reguillon, React. Chem. Eng. 4 (2019) 550–558.
[5] (a) L. Saputra, T. Kohima, T. Hara, N. Ichikuni, S. Shimazu, Mol. Catal. 453 (2018) 132–138;
(b) Y.Y. Li, A. Sabbaghi, J.L. Huang, K.C. Li, L.S. Tsui, F.L.Y. Lam, X.J. Hu, Mol. Catal. 485 (2020) 110789.
[6] (a) A. Dutta, M. Chetia, A.A. Ali, A. Bordoloi, P.S. Gehlot, A. Kumar, D. Sarma, Catal. Lett. 149 (2019) 141–150;
(b) E. Lagerapets, K. Lagerblom, E. Heliovaara, O.M. Hiltunen, K. Moslova, M. Nieger, T. Repo, Mol. Catal. 486 (2019) 75–79;
(c) A. Taher, D.W. Kim, I.M. Lee, RSC Adv. 7 (2017) 17806–17812;
(d) D.W. Tan, H.X. Li, M.J. Zhang, J.L. Yao, J.P. Lang, ChemCatChem 9 (2017) 1113–1118.
[7] Y.Y. Li, A. Chatterjee, L.B. Chen, F.L.Y. Lam, X.J. Hu, Mol. Catal. 488 (2020) 110869.
[8] X.J. Yang, Y.W. Zheng, L.Q. Zheng, L.Z. Wu, C.H. Tung, B. Chen, Green Chem. 21 (2019) 1401–1405.
[9] Y.K. Hu, L. Chen, B.D. Li, RSC Adv. 6 (2016) 65196–65204.
[10] Y.J. Li, B.S. Sun, W.J. Yang, Appl. Catal. A Gen. 515 (2016) 164–169.
[11] (a) J.L. Weber, I. Gugulan, P.E. de Jongh, K.P. de Jong, ChemCatChem. 10 (2018) 1107–1112;
(b) Y. Sohtome, Y. Hashimoto, K. Nagasawa, Eur. J. Org. Chem 13 (2006) 2894–2897.
[12] (a) L. Qian, Z.Y. Lu, T.H. Xu, X.C. Wu, Y. Tian, Y.P. Li, Z.Y. Huo, X.M. Sun, X. Duan, Adv. Energy Mater. 5 (2015) 1500245–1500250;
(b) S. Dresp, P. Strasser, ChemCatChem 10 (2018) 4162–4171.
[13] (a) M.Y. Wu, J.C. Mao, J. Guo, S.J. Ji, Eur. J. Org. Chem 23 (2008) 4050–4054;
(b) D. Padovan, A. Al-Nayili, C. Hammond, Green Chem. 19 (2017) 2846–2854;
(c) G. Morales, J.A. Melero, J. Iglesias, M. Paniagua, C. Lopez-Aguado, React. Chem. Eng. 4 (2019) 1834–1843.
[14] (a) F. Jiang, L. Zeng, S. Li, G. Liu, S.P. Wang, J.L. Gong, ACS Catal. 5 (2015) 438–447;
(b) M. Zhang, Y.J. Zhao, Q. Liu, L. Yang, G.L. Fan, F. Li, Dalton Trans. 45 (2016) 1093–1102;
(c) Y.J. Hong, X.Q. Yan, X.F. Liao, R.H. Li, S.D. Xu, L.P. Xiao, J. Fan, Chem. Commun. 50 (2014) 9679–9682;
(d) W.H. Luo, U. Deka, A.M. Beale, E.R.H. Van Eck, P.C.A. Bruijinincx, B.M. Weckhuysen, J. Catal. 301 (2013) 175–186.
[15] (a) J.M. Hoover, B.L. Ryland, S.S. Stahl, J. Am. Chem. Soc. 135 (2013) 2357–2367;
(b) C. Aellig, C. Girard, I. Hermans, Angew. Chem. Int. Ed 50 (2011) 12355–12360;
(c) J.C. Manayil, S. Sankaranarayanan, D.S. Bhadoria, K. Srinivasan, Ind. Eng. Chem. Res. 50 (2011) 13380–13386.
[16] (a) T. Mallat, A. Baiker, Chem. Rev. 104 (2004) 3037–3058;
(b) Q.J. Zhu, W.L. Dai, K.N. Fan, Green Chem. 12 (2010) 205–208.

[17] (a) H. Chen, S. He, M. Xu, M. Wei, D.G. Eyans, X. Duan, ACS Catal. 7 (2017) 2735–2743;
(b) T. Stoylkova, C. Chanev, Reac Kinet Mech Cat. 117 (2016) 47–58;
(c) J.P.H. Li, A.A. Adesina, E.M. Kennedy, M. Stockenhuber, Phys. Chem. Chem. Phys. 19 (2017) 26630–26644;
(d) H.B. Li, Y.Y. Cui, Q.Q. Liu, W.L. Dai, ChemCatChem. 10 (2018) 619–624;
(e) K. Motokura, M. Tada, Y. Iwasawa, Chem. Asian J. 3 (2008) 1230–1236.

[18] B. Helms, S.J. Guillaudeu, Y. Xie, M. McMurdo, C.J. Hawker, Frechet, Angew. Chem. Int. Ed. 44 (2005) 6384–6387.

[19] (a) P. Li, Y. Yu, P.P. Huang, H. Liu, C.Y. Cao, W.G. Song, J. Mater. Chem. A Mater. Energy Sustain. 2 (2014) 339–344;
(b) Y.R. Lee, Y.M. Chung, W.S. Ann, RSC Adv. 4 (2014) 23064–23067;
(c) X.Y. Xu, J.A. van Bokhoven, M. Ranocchiari, ChemCatChem 6 (2014) 1887–1891;
(d) W.K. Li, Z. Cai, Y. Shen, Y.Q. Zhu, H.C. Li, X.B. Zhang, F.M. Wang, Mol. Catal. 472 (2019) 17–26.

[20] B.Y. Li, Y.M. Zhang, D.X. Ma, L. Li, G.H. Li, G.D. Li, Z. Shi, S.H. Feng, Chem. Commun. (Camb.) 48 (2012) 6151–6153.

[21] (a) J. Zhang, H. Wang, L. Wang, S. Ali, C.T. Wang, L.X. Wang, X.J. Meng, B. Li, D.S. Su, F.S. Xiao, J. Am. Chem. Soc. 141 (2019) 2975–2983;
(b) T.R. Cook, P.J. Stang, Chem. Rev. 115 (2015) 7001–7045;
(c) S. Herrmann, E. Iglesia, J. Catal. 360 (2018) 66–80;
(d) J.D. Bass, A. Katz, Chem. Mater. 18 (2006) 1611–1620.

[22] M.L. Cai, X.Z. Wang, Y.Q. Chen, L.Y. Dai, Mol. Catal. 480 (2020) 110643–110650.

[23] (a) C. Xu, L. Zhang, Y. An, X.Z. Wang, G. Xu, Y.Q. Chen, L.Y. Dai, Appl. Catal. A Gen. 558 (2018) 26–33;
(b) X.T. Su, F. Xiao, Y.N. Li, J.K. Jian, Q.J. Sun, J.D. Wang, Mater. Lett. 64 (2010) 1232–1234.

[24] (a) E. Weber, D. Levy, M. Ben Sasson, A.N. Fitch, B. Pokroy, RSC Adv. 5 (2015) 98626–98633;
(b) G.V. Itina, A.A. Davydov, M.A. Osipova, L.N. Kurina, React. Kinet. Catal. Lett. 45 (1991) 243–249.

[25] G.A. Babu, G. Ravi, Mater. Lett. 161 (2015) 149–152.

[26] X. Wang, J.S. Tian, Y.H. Zheng, X.L. Xu, W.M. Liu, ChemCatChem 6 (2014) 1604–1611.

[27] H.T. Xu, W.J. Liu, Y. Zhao, D. Wang, J.Z. Zhao, J. Colloid Interface Sci. 540 (2019) 585–592.

[28] T. Zhang, Z.L. Zhu, H.N. Chen, Y. Bai, S. Xiao, X.L. Zheng, Q.Z. Xue, S.H. Yang, Nanoscale 7 (2015) 2933–2940.

[29] (a) J. Barrault, M. Boulinguiez, C. Forquy, R. Maurel, Appl. Catal. 33 (1987) 309–330;
(b) X.Y. Xu, S.M. Liu, Y. Cui, X.T. Wang, K. Smith, Y.J. Wang, Catalysts 9 (2019) 389–400.

[30] (a) Q.Q. Wang, S.H. Xu, F.L. Shen, Appl. Surf. Sci. 257 (2011) 7671–7677;
(b) H.T. Cui, G.Y. Hong, Chin J Appl Chem. 18 (2001) 208–211.

[31] K.S.W. Sing, Pure Appl. Chem. 54 (1982) 2201–2218.

[32] K. Shimizu, K. Kon, K. Shimura, S.S.M.A. Hakim, J. Catal. 300 (2013) 242–250.

[33] (a) L. He, Y.Q. Huang, A.Q. Wang, Y. Liu, X.Y. Liu, X.W. Chen, J.J. Delgado, X.D. Wang, T. Zhang, J. Catal. 298 (2013) 1–9;
(b) K. Na, S. Alayoglu, R. Ye, G.A. Somorjai, J. Am. Chem. Soc. 136 (2014) 17207–17212.

[34] (a) R. Debek, M. Radlik, M. Motak, M.E. Galvez, W. Turek, P. Da Costa, T. Graybek, Catal. Today 257 (2015) 59–65;
(b) V.K. Diez, C.R. Apesteguia, J.I. Di, Cosimo, J. Catal. 240 (2006) 235–244.

[35] (a) D.P. Depuccio, L. Ruiz-Rodriguez, E. Rodriguez-Castellon, P. Botella, J.M.L. Nieto, C.C. Landry, J. Phys. Chem. C 120 (2016) 27954–27963;
(b) Y. Peng, W.Z. Si, X. Li, J.J. Chen, J.H. Li, J. Crittenden, J.M. Hao, Environ. Sci. Technol. 50 (2016) 9576–9582;
(c) M. Iwasaki, E. Iglesia, J. Catal. 342 (2016) 84–97.

[36] (a) B. Mei, A. Becerikli, A. Pougin, D. Heesken, I. Sinev, W. Grunert, M. Muhler, J. Strunk, J. Phys. Chem. C. 116 (2012) 14318–14372;
(b) A. Auroux, A. Gervasini, J. Phys. Chem. 94 (1990) 6371–6379;
(c) X.Y. Xia, J. Strunk, W. Busser, R.N. d'Alnoncourt, M. Muhler, J. Phys. Chem. C. 112 (2008) 10938–10942;
(d) H. Vinek, J. Lercher, H. Noller, React. Kinet. Catal. Lett. 15 (1980) 21–25;
(e) V. Akula, K. Vankudoth, A.H. Padmasri, R. Sarkari, V.K. Velisoju, N. Gutta, N.K. Sathu, C.N. Rohita, New J. Chem. 41 (2017) 9875–9883.

[37] W.H. Luo, W.X. Cao, P.C.A. Bruijinincx, L. Lin, A.Q. Wang, T. Zhang, Green Chem. 21 (2019) 3744–3768.

[38] (a) G.B. Payne, P.H. Williams, P.H. Deming, J. Org. Chem. 26 (1961) 659–663;
(b) D. Limnios, C.G. Kokotos, J. Org. Chem. 79 (2014) 4270–4276;
(c) K. Yamaguchi, T. Mizugaki, K. Editani, K. Kaneda, New J. Chem. 23 (1999) 799–801.

[39] (a) B. Karimi, F.B. Rostami, M. Khorasani, D. Elhamifar, H. Vali, Tetrahedron 70 (2014) 6114–6119;
(b) X.F. Guo, L. Tang, Y. Yang, Z.G. Zha, Z.Y. Wang, Green Chem. 16 (2014) 2443–2447.

[40] M.J. Frisch, G.W. Trucks, H.B. Schlegel, G.E. Scuseria, M.A. Robb, J.R. Cheeseman, G. Scalmani, V. Barone, B. Mennucci, G.A. Petersson, H. Nakatsuji, M. Caricato, X. Li, H.P. Hratchian, A.F. Izmaylov, J. Bloino, G. Zheng, J.L. Sonnenberg, M. Hada, M. Ehara, K. Toyota, R. Fukuda, J. Hasegawa, M. Ishida, T. Nakajima, Y. Honda, O. Kitao, H. Nakai, T. Vreven, J.A. Montgomery Jr, J.E. Peralta, F. Ogliaro, M. Bearpark, J.J. Heyd, E. Brothers, K.N. Kudin, V.N. Staroverov, T. Keith, R. Kobayashi, J. Normand, K. Raghavachari, A. Rendell, J.C. Burant, S.S. Iyengar, J. Tomasi, M. Cossi, N. Rega, J.M. Millam, M. Klene, J.E. Knox, J.B. Cross, V. Bakken, C. Adamo, J. Jaramillo, R. Gomperts, R.E. Stratmann, O. Yazyev, A.J. Austin, R. Cammi, C. Pomelli, J.W. Ochterski, R.L. Martin, K. Morokuma, V.G. Zakrzewski, G.A. Voth, P. Salvador, J.J. Dannenberg, S. Dapprich, A.D. Daniels, O. Farkas, J.B. Foresman, J.V. Ortiz, J. Cioslowski, D.J. Fox, Gaussian 09., Revision D.01.01, Gaussian, Inc., Wallingford CT, 2013.

[41] (a) H. Chen, S. He, M. Xu, M. Wei, D.G. Eyans, X. Duan, ACS Catal. 7 (2017) 2735–2743;
(b) Y. Liu, X.C. Ma, G.G. Chang, S.C. Ke, T. Xia, Z.Y. Hu, X.Y. Yang, J. Colloid. Interf. Sci. 557 (2019) 207–215.

[42] (a) T. Tatsumi, Y. Watanabe, Y. Hirasawa, J. Tsuchiya, Res. Chem. Intermed. 24 (1998) 529–540;
(b) K. Rajabimoghadam, Y. Darwish, U. Bashir, D. Pitman, S. Eichelberger, M.A. Siegler, M. Swart, I. Garcia-Bosch, J. Am. Chem. Soc. 140 (2018) 16625–16634;
(c) F. Mecozzi, J.J. Dong, P. Saisaha, W.R. Browne, Eur. J. Org. Chem. 46 (2017) 6919–6925.

[43] (a) Y.F. Zhu, Y.L. Zhu, G.Q. Ding, S.H. Zhu, H.Y. Zheng, Y.W. Li, Appl. Catal. A Gen. 468 (2013) 296–304;
(b) H.R. Yue, Y.J. Zhao, X.B. Ma, J.L. Gong, Chem. Soc. Rev. 41 (2012) 4218–4244;
(c) S. Shylesh, W.R. Thiel, ChemCatChem 2 (2011) 278–287;
(d) P. Saisaha, J.J. Dong, T.G. Meinds, J.W. de Boer, R. Hage, F. Mecozzi, J.B. Kasper, W.R. Browne, ACS Catal. 6 (2016) 3486–3495;
(e) S. Mondal, H. Malviya, P. Biswas, React. Chem. Eng. 4 (2019) 595–609.